communications materials

Article

https://doi.org/10.1038/s43246-024-00554-9

Particle-hole mixed Bogoliubov quasiparticles and Cooper instability in single-unit-cell FeSe/$SrTiO_3$ films

Zhiyuan Wei[1,5], Shaozhi Li[2,5], Bo Liu[1], Xiupeng Sun[1], Yinqi Hu[1], Shuai Sun[1], Shuting Peng[1], Yang Luo[1], Linwei Huai[1], Jianchang Shen[1], Bingqian Wang[1], Yu Miao[1], Zhipeng Ou[1], Yao Wang[2,3], Kun Jiang[4] & Junfeng He[1]

In conventional superconductors, Bogoliubov quasiparticles and Cooper instability provide a paradigm to describe the superconducting state and the superconducting transition, respectively. However, whether these concepts can be adapted to describe Fe-based superconductors requires rigorous examinations from experiments. Here, we report angle-resolved photoemission studies on single-layer FeSe films grown on $SrTiO_3$ substrate. Due to the improved clarity, our results reveal both particle and hole branches of the energy band with clear quasiparticles. The dispersion and coherence factors are extracted, which unveil the particle-hole mixed Bogoliubov quasiparticles in the superconducting state of the FeSe/STO films. Effective pairing susceptibility is also deduced as a function of temperature, which indicates the persistence of Cooper instability in Fe-based superconductors.

An important step towards understanding high-temperature superconductors is to correctly describe their superconducting state. In conventional superconductors, the superconducting state is described by Bogoliubov quasiparticles of the Bardeen–Cooper–Schrieffer (BCS) theory[1,2]. The BCS-Bogoliubov quasiparticles represent a coherent combination of electrons and holes, giving rise to a particle–hole symmetric band dispersion with a spectral weight distribution described by the BCS-coherence factors[1,2]. However, the superconducting state in correlated materials may deviate from the conventional picture at least via three routes. First, strong electron correlation and competing states in selected superconductors may invalidate the concept of quasiparticles[3–7]. Second, quasiparticles may survive in superconductors with moderate correlation, but the particle–hole symmetry of the band dispersion would be broken if Cooper pairs are formed with a finite net momentum[8–10]. Third, the particle–hole symmetric band dispersion may also persist in some correlated superconductors, while the spectral weight distribution exhibits a substantial difference from that of the BCS-coherence factors[11–14]. It has been proposed that the superconducting state in selected correlated superconductors would inherit the non-Fermi liquid characters of their strange normal states[11].

Another fundamental issue in high-temperature superconductors is to understand how the superconducting phase transition takes place. In the BCS theory, the probability of electrons forming Cooper pairs has a log singularity as the temperature decreases. This Cooper instability arises from the Fermi liquid normal state, which would eventually drive the superconducting phase transition[1,15]. However, the normal state of correlated high-temperature superconductors could be non-Fermi liquid, where multiple intertwined or competing orders may also exist. As such, the Cooper log instability for superconductivity might disappear, and alternative pairing instabilities may take place[16].

In cuprate high-temperature superconductors, the descriptions of both superconducting state and superconducting phase transition have been systematically investigated[16–19]. BCS-like Bogoliubov quasiparticles have been reported in the superconducting state of overdoped $Bi_2Sr_2Ca_2Cu_3O_{10+\delta}$[17] and nearly optimal-doped $Bi_2Sr_2CaCu_2O_{8+\delta}$[18], while deviations from the BCS description have been suggested in the underdoped regime[12]. The Cooper log instability is proposed to drive the superconducting transition in overdoped cuprates, but this instability disappears in samples with the pseudo-gapped non-Fermi liquid normal state[16]. These results have placed clear constraints on the superconducting mechanism in cuprates. Therefore, it is necessary to perform a similar investigation on Fe-based superconductors, the second family of high-temperature superconductors. The electron correlation is moderate in Fe-based

[1]Department of Physics and CAS Key Laboratory of Strongly-coupled Quantum Matter Physics, University of Science and Technology of China, Hefei, Anhui, China. [2]Department of Physics and Astronomy, Clemson University, Clemson, SC, USA. [3]Department of Chemistry, Emory University, Atlanta, GA, USA. [4]Beijing National Laboratory for Condensed Matter Physics and Institute of Physics, Chinese Academy of Sciences, Beijing, China. [5]These authors contributed equally: Zhiyuan Wei, Shaozhi Li. e-mail: jfhe@ustc.edu.cn

superconductors, but non-Fermi liquid behaviors have been widely reported[20–24]. These non-Fermi liquid behaviors lead to a naïve question about the validity of the BCS descriptions of both superconducting state and superconducting phase transition in Fe-based superconductors. Technically, an experimental challenge in fully revealing the superconducting state of Fe-based superconductors is associated with the relatively lower superconducting transition temperature (T_c). In principle, a quantitative evaluation requires both particle and hole branches of the electronic structure in the superconducting state[17,18], but the lower T_c hampers the observation of the hole branch above Fermi level (E_F) by thermal population in photoemission measurements.

In this article, we report angle-resolved photoemission spectroscopy (ARPES) measurements on single-unit-cell (1UC) FeSe films grown on $SrTiO_3$ substrate (FeSe/STO), in which relatively large electron correlation is reported[25,26] and the superconducting gap persists to the highest temperature among the Fe-based superconductors at ambient pressure[26–34]. By improving the quality of the films and the clarity of the ARPES data, we have revealed both particle and hole branches of the band dispersion, as well as their spectral weight distribution as a function of momentum. The coherence factors are extracted, which agree with that of the BCS-Bogoliubov quasiparticles. Bogoliubov angle is also determined, which directly reveals the particle–hole dualism in the system. Effective pairing susceptibility is deduced as a function of temperature, indicating the persistence of Cooper instability in this system.

Results

BCS simulation and electronic structure

We start with a standard BCS superconducting state to illustrate that both the particle–hole symmetric band dispersion and the BCS-coherence factors can be revealed by the spectral function $A(\boldsymbol{k}, \omega)$. First, the particle–hole symmetric dispersion is directly seen in an intensity plot of the $A(\boldsymbol{k}, \omega)$ (Fig. 1a), which can be further quantified by a waterfall plot of the energy distribution curves (EDCs) near the Fermi momentum (Fig. 1b). Second, the Bogoliubov quasiparticle excitations in the superconducting state are a linear combination of particles and holes with coherence factors $u_{\boldsymbol{k}}$ and $v_{\boldsymbol{k}}$, which are connected to $A(\boldsymbol{k}, \omega)$ by

$$A(\boldsymbol{k}, \omega > 0) = \left|u_{\boldsymbol{k}}\right|^2 \delta(\omega - E_{\boldsymbol{k}}), A(\boldsymbol{k}, \omega < 0) = \left|v_{\boldsymbol{k}}\right|^2 \delta(\omega + E_{\boldsymbol{k}}),$$

where $E_{\boldsymbol{k}}$ and $-E_{\boldsymbol{k}}$ are the dispersion above and below the Fermi energy E_F, respectively. Therefore, the coherence factors can be directly extracted from $A(\boldsymbol{k}, \omega)$, which satisfy the following relations in the BCS superconducting state (Fig. 1c)

$$\left|u_{\boldsymbol{k}}\right|^2 = \frac{1}{2}\left(1 + \frac{\varepsilon_{\boldsymbol{k}}}{E_{\boldsymbol{k}}}\right), \left|v_{\boldsymbol{k}}\right|^2 = \frac{1}{2}\left(1 - \frac{\varepsilon_{\boldsymbol{k}}}{E_{\boldsymbol{k}}}\right),$$

where $\varepsilon_{\boldsymbol{k}}$ is the bare band dispersion in the normal state.

In order to examine the superconducting state of the 1UC FeSe/STO film, high-resolution ARPES measurements have been carried out to probe the spectral function $A(\boldsymbol{k}, \omega)$. Electron-like bands are revealed along a high symmetry cut across the M $(-\pi, -\pi)$ point (Fig. 2a). The splitting of energy bands with different orbitals[35] is clearly revealed in the raw data (Fig. 2b), demonstrating the high quality of the FeSe/STO film. The superconducting gap shows different gap size on bands with different orbitals, which disappears at ~65 K (Fig. 2c, d), being consistent with the earlier studies[30,33,36]. The back-bending of the bands due to superconducting gap opening is also observed (Fig. 2b). In principle, one can compare the curvature of the back-bending dispersion with that of the BCS-Bogoliubov quasiparticles. As shown in Fig. 2b, our results are largely consistent with the calculated band dispersions (also see Supplementary Note 1 and Supplementary Fig. 1). Nevertheless, we note that debates have been raised on the curvature analysis of the electron-like band below E_F (occupied branch)[36,37], possibly due to the limited back-bending region for the quantitative analysis. In this regard, the examination of the unoccupied branch above E_F is important. With an improved quality of the film, the energy band above E_F is indeed resolved at elevated temperatures (Fig. 2e–k, also see Supplementary Note 2 and Supplementary Fig. 2). This observation provides an opportunity to quantitatively examine both the particle–hole band dispersion and the BCS-coherence factors.

Particle–hole mixed Bogoliubov quasiparticles

Quantitative analysis of both particle and hole branches has been carried out at a moderate temperature (47 K), where the superconducting gap still persists (Fig. 3). To avoid the complication of the band splitting, we take advantage of the ARPES matrix element effect which selectively probes the inner branch of the electron-like band (Fig. 3b, c) along the high symmetry cut across the $(-\pi, \pi)$ point (Fig. 3a). Fermi-Dirac function is removed to reveal the branch above E_F due to the thermal population. We note that the accurate determination of the Fermi level, energy resolution, and the correct subtraction of the background are important for the analysis. We have followed the typical process used in cuprates, and the details are elaborated in Supplementary Notes 3–5 (Supplementary Figs. 3–8). As shown in Fig. 3e, two peaks can be seen in the raw energy distribution curves (EDCs) near the Fermi momentum $\boldsymbol{k}_F$. Following the analysis in cuprates[17,18], two equal-width Lorentzians are used to fit each EDC in an energy window near E_F (Fig. 3e). The peak position shows the two branches of dispersion, and the peak height reflects the coherence factors[17,18]. In Fig. 3g, we summarize the extracted coherence factors $|u_{\boldsymbol{k}}|^2$ and $|v_{\boldsymbol{k}}|^2$, which are qualitatively consistent with that calculated for the BCS-Bogoliubov quasiparticles. The sum of $|u_{\boldsymbol{k}}|^2$ and $|v_{\boldsymbol{k}}|^2$ remains a constant as a function of momentum within the experimental error bars. We have also extracted the Bogoliubov angle $\Theta_{\boldsymbol{k}} = \arctan[(\frac{|u(\boldsymbol{k})|^2}{|v(\boldsymbol{k})|^2})^{\frac{1}{2}}]$, which describes the mixture between particles and holes[18]. As shown in Fig. 3h, the $\Theta_{\boldsymbol{k}}$ gradually increases as a function of momentum with a value of 45° at $\boldsymbol{k}_F$. This is similar to that observed in cuprates[18], indicating a continuous evolution of particle–hole mixing with an equal mixing ratio at $\boldsymbol{k}_F$. For comparison, the raw EDCs in the normal state (87 K) are also examined (Fig. 3d, f), where only one peak is identified, either below ($|v_{\boldsymbol{k}}|^2 = 1, \left|u_{\boldsymbol{k}}\right|^2 = 0$) or above ($|v_{\boldsymbol{k}}|^2 = 0, \left|u_{\boldsymbol{k}}\right|^2 = 1$) the E_F. Therefore, the Bogoliubov angle is either 0° or 90° with a sudden jump around $\boldsymbol{k}_F$ (Fig. 3h), demonstrating the absence of particle–hole mixing.

Pairing instability

After revealing the superconducting state, we next examine the pairing instability that drives the superconducting transition. Systematic measurements have been carried out to quantify the evolution of the spectral function $A(\boldsymbol{k}, \omega)$ as the temperature decreases towards the superconducting transition (Fig. 4). Following the analysis in cuprates[16,19], we can directly calculate the effective pairing susceptibility χ from the measured spectral function $A(\boldsymbol{k}, \omega)$ via the equation

$$\chi = \int \frac{d^3\boldsymbol{k}}{(2\pi)^3} \int \frac{d\omega}{2\pi} \int \frac{d\omega'}{2\pi} A(-\boldsymbol{k}, \omega) A(\boldsymbol{k}, \omega') \frac{1 - f(\omega) - f(\omega')}{\omega + \omega'},$$

where $f(\omega)$ is the Fermi-Dirac distribution function (see Supplementary Note 6 and Supplementary Eqs. (1–7) for the details). Theoretically, the integral covers the entire momentum and energy space. Due to the reduced contributions away from the Fermi momentum and energy, we evaluate this integral from experimental data over a large momentum and energy window (indicated by the red box in the inset of Fig. 4c). The extracted effective pairing susceptibility exhibits a logarithmical behavior as a function of temperature, pointing to a tendency towards superconducting phase transition (Fig. 4c). This is fully consistent with the existence of Cooper instability in the FeSe/STO film. In order to perform a comparison between various Fe-based superconductors and cuprates, the integral over $\boldsymbol{k}$ is now simplified by taking $\boldsymbol{k} = \boldsymbol{k}_F$, as χ is dominated by the spectral weight at $\boldsymbol{k}_F$[19] (see Supplementary Eq. (7)). The simplified pairing susceptibility, denoted

as χ_F, is extracted from the reported electronic structure of Fe-based superconductors[38,39] and presented with that from the cuprates[19]. The temperature dependence of the extracted χ_F remains similar in various Fe-based superconductors, but it is distinct from that in the optimally doped cuprates (Fig. 4d) (also see Supplementary Note 7, Supplementary Fig. 9 and related discussions on the slope of the effective pairing susceptibility).

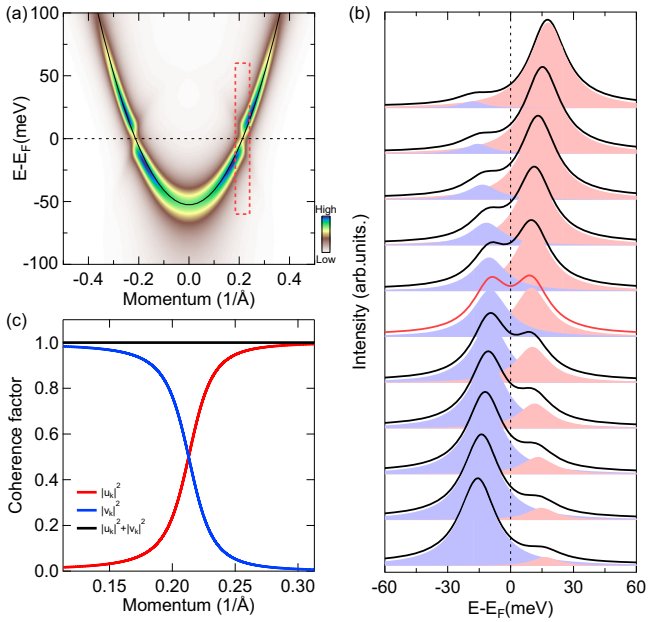

Fig. 1 | Simulation of BCS superconducting state. a Intensity plot of the simulated spectral function A(**k**, ω). **b** EDCs extracted from the red-boxed area in (**a**). **c** Coherence factors as a function of momentum in the red-boxed area in (**a**). A bare band extracted from the normal state of the 1UC FeSe/STO film is used for the simulation, which is shown by the black line in (**a**). A superconducting gap of 10 meV is considered in the simulation.

Discussion

Finally, we discuss the implications of our experimental observations. As the second material family with unconventional high-temperature superconductivity, the Fe-based superconductors exhibit many behaviors which are different from the prediction of the conventional BCS theory[20–24,26,28]. However, our experimental observations, including the particle–hole mixing, coherence factors, and Bogoliubov angles, demonstrate that the BCS description remains valid for the superconducting state near E_F in the FeSe/STO film. We note that electron correlation is a key constituent that may give rise to a superconducting state different from that of the BCS description, and the FeSe/STO film shows relatively strong electron correlations among all the Fe-based superconductors[25,26]. In this regard, our results may provide more general insights into the superconducting state in other Fe-based superconductors.

The extracted effective pairing susceptibility reveals a temperature dependence describable by the Cooper log instability, indicating that a small attractive interaction would drive a low-temperature superconductivity phase transition in the Fe-based superconductors. This is different from that in the optimally doped cuprates (Fig. 4d), where the Cooper instability is likely to be suppressed by the pseudo-gapped non-Fermi liquid normal state[16]. In the context of Fe-based superconductors, while contributions from various bosonic fluctuations to the pairing interaction are still an open question, our discovery of the Cooper log instability provides a strong constraint on the pairing mechanism: if the temperature dependence of this bosonic media can be ignored below T_c, the pairing interaction should be limited to a thick shell around the Fermi surface. While such a truncation in the effective energy range of this pairing interaction is similar to the Debye frequency of phonons, the existence of Cooper log instability does not rely on a particular pairing mechanism, and the pairing mechanism in Fe-based superconductors can still be unconventional.

In summary, we have systematically investigated ARPES measurements on the 1UC FeSe/STO films with improved quality. Our results have experimentally established the basic descriptions of the superconducting state of the FeSe/STO films, as well as the superconducting phase transition in several Fe-based superconductors. Future studies are stimulated to investigate the interplay between the reported non-Fermi liquid

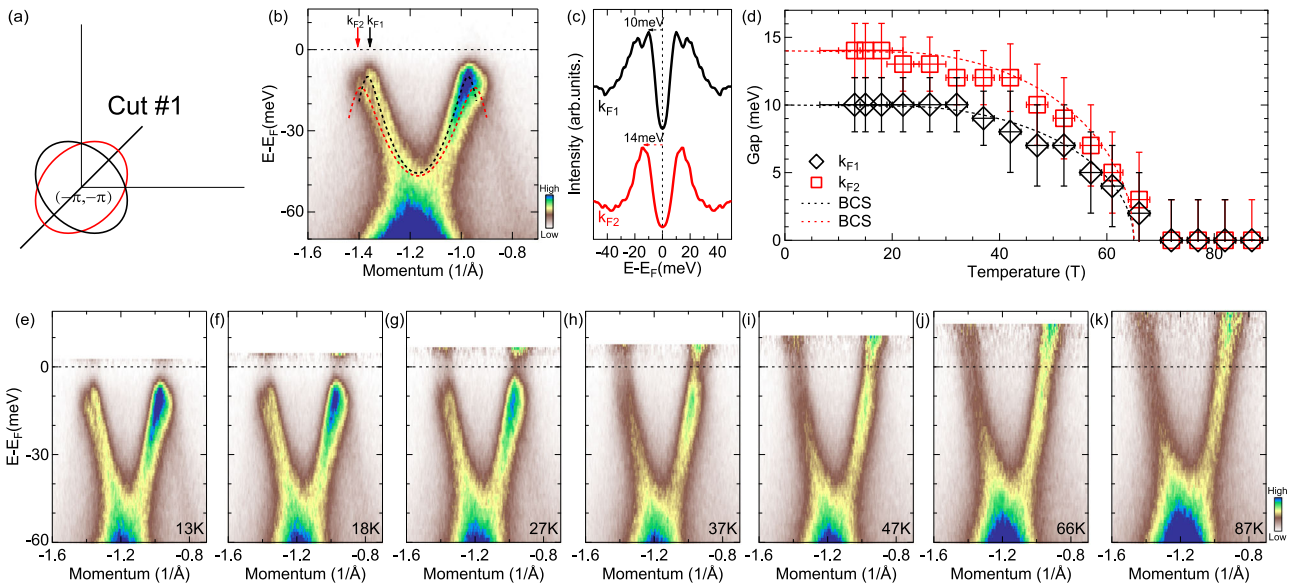

Fig. 2 | Observation of both particle and hole branches of the band dispersion. a Location of the momentum cut (#1) in the Brillouin zone. **b** Photoemission intensity plot of the band along cut #1 at 13 K. The split bands are marked by the black and red dashed lines, and the Fermi momenta of the two bands are marked as $\mathbf{k}_{F_1}$ and $\mathbf{k}_{F_2}$, respectively. **c** Symmetrized EDC at $\mathbf{k}_{F_1}$ ($\mathbf{k}_{F_2}$) is shown in black (red). The different gap sizes are labeled. **d** Temperature dependence of the superconducting gap at $\mathbf{k}_{F_1}$ (black diamonds) and $\mathbf{k}_{F_2}$ (red squares). BCS fittings are shown by the dashed lines. The vertical (horizontal) error bars represent the uncertainties in the determination of the gap (temperature). **e**–**k** Fermi-Dirac divided photoemission intensity plot of the band along cut #1 at 13 K, 18 K, 27 K, 37 K, 47 K, 66 K, and 87 K, respectively.

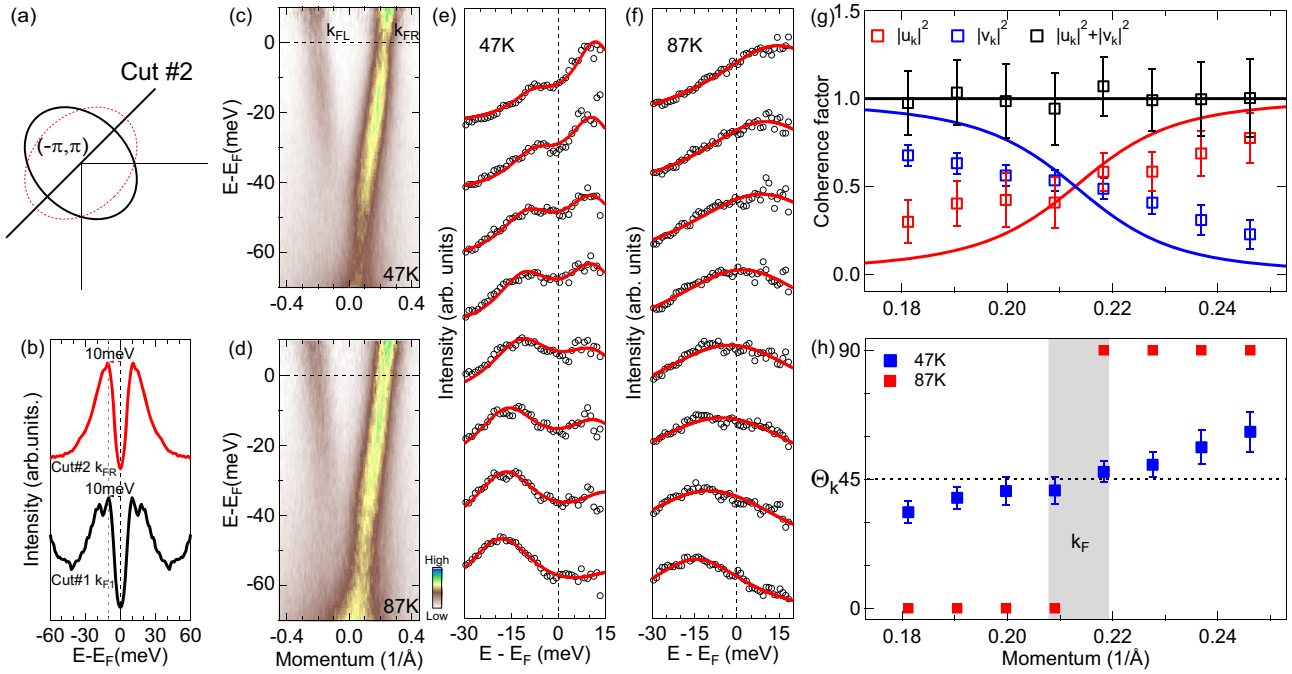

Fig. 3 | Particle–hole mixing band structure in the 1UC FeSe/STO film. a Location of the momentum cut (#2) in the Brillouin zone. **b** Comparison between the EDC at the Fermi momentum (k_{FR}) of cut #2 (red) and the EDC at the Fermi momentum (k_{F_1}) of cut #1 (black, same as that in Fig. 2c). **c**, **d** Fermi-Dirac divided photoemission intensity plot of the band measured along cut #2 at 47 K and 87 K, respectively. **e**, **f** Raw EDCs (black) and fitting results (red) in the momentum region near $\mathbf{k}_F$, measured at 47 K and 87 K, respectively. **g** Extracted coherence factors. $|v_\mathbf{k}|^2$ ($|u_\mathbf{k}|^2$) represents the coherence factor for the branch below (above) E_F. The simulated BCS-coherence factors are plotted as solid lines. **h** Extracted Bogoliubov angle at 47 K (blue) and 87 K (red). The error bars represent the uncertainties in the determination of the coherence factors and the Bogoliubov angle.

Fig. 4 | Effective pairing susceptibility extracted from the experiments. a schematic of Cooper log instability from a Fermi liquid normal state, where the pairing probability increases logarithmically as the temperature decreases towards the superconducting T_c. **b** schematic of an opposite case in a special non-Fermi liquid system, where the pairing probability decreases when the temperature decreases. **c** Extracted effective pairing susceptibility as a function of temperature for the FeSe/STO film. The integral window is shown by the red box in the inset. The gray line represents a logarithmical fit $[\ln(\frac{1}{T})]$ to the experimental data. **d** Simplified effective pairing susceptibility from scatterings of electrons at $\mathbf{k}_F$ (indicated by the black arrow in (**c**)) as a function of temperature for the FeSe/STO film, LiFeAs[38], $K_xFe_{2-y}Se_2$[39], overdoped $Bi_2Sr_2CaCu_2O_{8+\delta}$ (Bi-2212) and optimally doped $Bi_2Sr_2CuO_{6+\delta}$ (Bi-2201)[19]. For comparison, the absolute value at each temperature is normalized by that at the highest temperature.

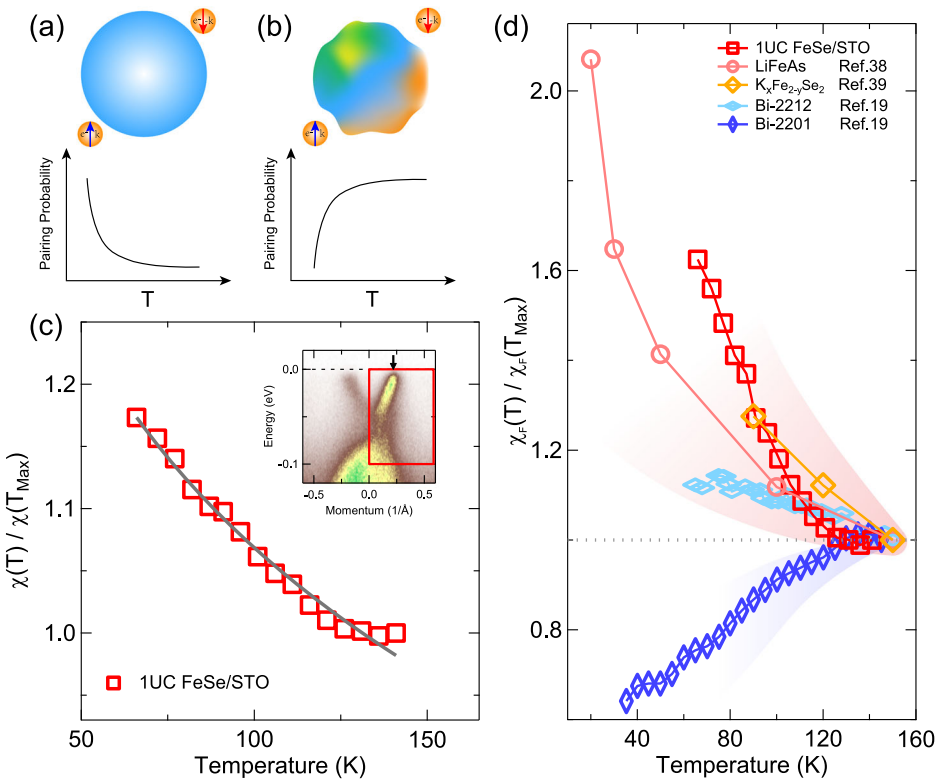

behaviors[20–24], the BCS-like superconducting state and the Cooper-instability-driven phase transition in Fe-based superconductors.

Methods

Sample growth and ARPES measurements

High-quality FeSe/STO films were grown by molecular beam epitaxy (MBE) on Nb-doped $SrTiO_3$ substrates. The substrates were prepared following the previous method[40], and kept at 570 °C during the growth. Se (99.999%) and Fe (99.995%) were evaporated onto the substrates at a flux ratio of ~10:1 for 18 min. After the growth, the films were annealed at 660 °C for 8 h. The base pressure of the MBE chamber was better than 6×10^{-11} torr. ARPES measurements were carried out in our lab-based ARPES system, which was directly connected to the MBE chamber. The total energy resolution was ~4 meV, and the base pressure was better than 5×10^{-11} torr. A photon energy of 21.2 eV was used in the measurements, and the Fermi level was determined by measuring a polycrystalline Au specimen in electrical contact with the samples.

Data availability

The raw data generated in this study are provided in the article and the supplementary materials.

Received: 10 January 2024; Accepted: 21 June 2024;
Published online: 06 July 2024

References

1. Bardeen, J., Cooper, L. N. & Schrieffer, J. R. Theory of superconductivity. *Phys. Rev.* **108**, 1175–1204 (1957).
2. Bogoliubov, N. N. On a new method in the theory of superconductivity. *Nuovo Cimento* **7**, 794–805 (1958).
3. Campuzano, J. C. et al. Electronic spectra and their relation to the (π, π) collective mode in high-T_c superconductors. *Phys. Rev. Lett.* **83**, 3709 (1999).
4. Feng, D. L. et al. Signature of superfluid density in the single-particle excitation spectrum of $Bi_2Sr_2CaCu_2O_{8+\delta}$. *Science* **289**, 277–281 (2000).
5. Tanaka, K. et al. Distinct Fermi-momentum-dependent energy gaps in deeply underdoped Bi2212. *Science* **314**, 1910–1913 (2006).
6. Zhao, J. J. et al. Universal features in the photoemission spectroscopy of high-temperature superconductors. *Proc. Natl. Acad. Sci. USA* **110**, 17774–17777 (2013).
7. Drozdov, I. K. et al. Phase diagram of $Bi_2Sr_2CaCu_2O_{8+\delta}$ revisited. *Nat. Commun.* **9**, 5210 (2018).
8. Fulde, P. & Ferrell, R. A. Superconductivity in a strong spin-exchange field. *Phys. Rev.* **135**, A550 (1964).
9. Larkin, A. & Ovchinnikov, Y. N. Nonuniform state of superconductors. *Zh. Eksperim. i Teor. Fiz*. **47**, 1136–1146 (1964).
10. Kanasugi, S. & Yanase, Y. Anapole superconductivity from PT-symmetric mixed-parity interband pairing. *Commun. Phys.* **5**, 39 (2022).
11. Phillips, P. W., Yeo, L. & Huang, E. W. Exact theory for superconductivity in a doped Mott insulator. *Nat. Phys.* **16**, 1175–1180 (2020).
12. Randeria, M., Sensarma, R., Trivedi, N. & Zhang, F.-C. Particle-hole asymmetry in doped Mott insulators: implications for tunneling and photoemission spectroscopies. *Phys. Rev. Lett.* **95**, 137001 (2005).
13. Zou, C. W. et al. Particle–hole asymmetric superconducting coherence peaks in overdoped cuprates. *Nat. Phys.* **18**, 551–557 (2022).
14. Shaginyan, V. R., Msezane, A. Z., Japaridze, G. S. & Stephanovich, V. A. Violation of the time-reversal and particle-hole symmetries in strongly correlated fermi systems: a review. *Symmetry* **12**, 1596 (2020).
15. Cooper, L. N. Bound electron pairs in a degenerate Fermi gas. *Phys. Rev.* **104**, 1189–1190 (1956).
16. Maier, T. A. et al. Pairing in a dry Fermi sea. *Nat. Commun.* **7**, 11875 (2016).
17. Matsui, H. et al. BCS-like Bogoliubov quasiparticles in high-T_c superconductors observed by angle-resolved photoemission spectroscopy. *Phys. Rev. Lett.* **90**, 217002 (2003).
18. Balatsky, A. V., Lee, W. S. & Shen, Z. X. Bogoliubov angle, particle-hole mixture, and angle-resolved photoemission spectroscopy in superconductors. *Phys. Rev. B* **79**, 020505 (2009).
19. He, Y. *Spectroscopic Studies on Electronic Correlation and Lattice Coupling in Hole-Doped High-T_c Cuprates* (Stanford University, 2018).
20. Aichhorn, M., Biermann, S., Miyake, T., Georges, A. & Imada, M. Theoretical evidence for strong correlations and incoherent metallic state in FeSe. *Phys. Rev. B* **82**, 064504 (2010).
21. Kasahara, S. et al. Evolution from non-Fermi-to Fermi-liquid transport via isovalent doping in $BaFe_2(As_{1-x}P_x)_2$ superconductors. *Phys. Rev. B* **81**, 184519 (2010).
22. Dai, Y. M. et al. Spin-fluctuation-induced non-fermi-liquid behavior with suppressed superconductivity in $LiFe_{1-x}Co_xAs$. *Phys. Rev. X* **5**, 031035 (2015).
23. Xing, L. Y. et al. Observation of non-Fermi liquid behavior in hole-doped $LiFe_{1-x}V_xAs$. *Phys. Rev. B* **94**, 094524 (2016).
24. Huang, J. W. et al. Emergence of superconductivity from fully incoherent normal state in an iron-based superconductor $(Ba_{0.6}K_{0.4})Fe_2As_2$. *Sci. Bull.* **64**, 11–19 (2019).
25. Mandal, S., Zhang, P., Ismail-Beigi, S. & Haule, K. How correlated is the FeSe/$SrTiO_3$ system? *Phys. Rev. Lett.* **119**, 067004 (2017).
26. He, J. F. et al. Electronic evidence of an insulator-superconductor crossover in single-layer FeSe/$SrTiO_3$ films. *Proc. Natl. Acad. Sci. USA* **111**, 18501–18506 (2014).
27. Si, Q. M., Yu, R. & Abrahams, E. High-temperature superconductivity in iron pnictides and chalcogenides. *Nat. Rev. Mater.* **1**, 16017 (2016).
28. Sobota, J. A., He, Y. & Shen, Z.-X. Angle-resolved photoemission studies of quantum materials. *Rev. Mod. Phys.* **93**, 025006 (2021).
29. Wang, Q.-Y. et al. Interface-induced high-temperature superconductivity in single unit-cell FeSe films on $SrTiO_3$. *Chin. Phys. Lett*. **29**, 037402 (2012).
30. He, S. L. et al. Phase diagram and electronic indication of high-temperature superconductivity at 65 K in single-layer FeSe films. *Nat. Mater.* **12**, 605–610 (2013).
31. Tan, S. Y. et al. Interface-induced superconductivity and strain-dependent spin density waves in FeSe/$SrTiO_3$ thin films. *Nat. Mater.* **12**, 634–640 (2013).
32. Lee, J. J. et al. Interfacial mode coupling as the origin of the enhancement of T_c in FeSe films on $SrTiO_3$. *Nature* **515**, 245–248 (2014).
33. Zhang, Y. et al. Superconducting gap anisotropy in monolayer FeSe thin film. *Phys. Rev. Lett.* **117**, 117001 (2016).
34. Liu, D. et al. Electronic origin of high-temperature superconductivity in single-layer FeSe superconductor. *Nat. Commun.* **3**, 931 (2012).
35. Lee, D.-H. What makes the T_c of FeSe/$SrTiO_3$ so high? *Chin. Phys. B* **24**, 117405 (2015).
36. Xu, Y. et al. Spectroscopic evidence of superconductivity pairing at 83 K in single-layer FeSe/$SrTiO_3$ films. *Nat. Commun.* **12**, 2840 (2021).
37. Nakayama, K., Shigekawa, K., Sugawara, K., Takahashi, T. & Sato, T. Unusual temperature evolution of quasiparticle band dispersion in electron-doped FeSe films. *Symmetry* **13**, 155 (2021).
38. Miao, H. et al. Orbital-differentiated coherence-incoherence crossover identified by photoemission spectroscopy in LiFeAs. *Phys. Rev. B* **94**, 201109 (2016).

39. Yi, M. et al. Observation of temperature-induced crossover to an orbital-selective Mott phase in $A_xFe_{2-y}Se_2$(A=K, Rb) superconductors. *Phys. Rev. Lett.* **110**, 067003 (2013).
40. Wang, M. et al. Molecular beam epitaxy of single unit-cell FeSe superconducting films on $SrTiO_3$(001). *Acta Phys. Sin.* **63**, 027401 (2014).

Acknowledgements

The authors thank I. Esterlis, Y. He, S.-D. Chen, Z. J. Xiang, Z. Y. Wang, T. Wu, and X. H. Chen for useful discussions. The work at the University of Science and Technology of China (USTC) was supported by international partnership program of the Chinese Academy of Sciences (Grant No. 123GJHZ2022035MI), the Fundamental Research Funds for the Central Universities (Nos. WK3510000015, WK3510000012), the National Natural Science Foundation of China (Nos. 12074358, 52261135638), the Innovation Program for Quantum Science and Technology (Grant No. 2021ZD0302802) and the USTC start-up fund. S.L. and Y.W. acknowledge support from the Air Force Office of Scientific Research Young Investigator Program under grant FA9550-23-1-0153 and computational resources from the National Energy Research Scientific Computing Center, a DOE Office of Science User Facility supported by the Office of Science of the U.S. Department of Energy under Contract No. DE-AC02-05CH11231 using NERSC award BESERCAP0027096.

Author contributions

J.H. initiated the research. Z.W. grew the sample and performed the ARPES experiments with guidance from J.H. and help from X.S., Y.H., S.S., S.P., Y.L., L.H., J.S., B.W., Y.M., and Z.O. S.L., Y.W., and K.J. provided theoretical guidance. Z.W., S.L., and B.L. analyzed the data. J.H. and Z.W. wrote the paper with inputs from all authors.

Competing interests

The authors declare no competing interests.

Additional information

Supplementary information The online version contains supplementary material available at https://doi.org/10.1038/s43246-024-00554-9.

Correspondence and requests for materials should be addressed to Junfeng He.

Peer review information *Communications Materials* thanks Alexander Kordyuk and the other, anonymous, reviewer(s) for their contribution to the peer review of this work. Primary Handling Editors: Nicola Poccia and Aldo Isidori.